Effect of Scandium on the Structure and Electrochemical Properties of $La_{1-x}Sc_xNi_{3.5}$ Alloy Electrodes

Zhijie Gao [1, †, 2]*, Bo Zhang* [2,†]*, He Bian* [1]

[1] Department of Chemistry and Chemical Engineering, Binzhou University, Binzhou 256600, PR China
[2] Zhengzhou Institute of Multipurpose Utilization of Mineral Resources, Chinese Academy of Geological Sciences, Zhengzhou, 450006, PR China
[†] These authors contributed equally to this work
*E-mail: gaozhijie1983@126.com

La-Sc-Ni based A_2B_7-type hydrogen storage alloys $La_{1-x}Sc_xNi_{3.5}$ (x = 0.0~1.0) is prepared by an arc furnace method and maintained for a week in a sealed stainless steel tube at 1173 K. XRD and SEM-EDS results show that the alloys are mainly consisted of $LaNi_5$, La_2Ni_7 and minor LaNi phases. Under appropriate amount of Sc addition (x = 0.3~0.5), the $(La, Sc)_2Ni_7$ phase increases whereas the $LaNi_5$ and LaNi phases decreases. Moreover, the further increase of Sc content results in appearance of Sc_2Ni_7 phase. The thermodynamic analyses show that the enthalpy change of $La_{0.7}Sc_{0.3}Ni_{3.5}$-H_2 is more close to -7.5 kcal mol^{-1} for the La-Mg-Ni-H_2 system while the equilibrium absorption/desorption hydrogen pressure plateau of that is still higher than La-Mg-Ni systems, which indicate that the phase rule of Sc-containing alloy is different from Mg-containing alloy. Compared to pure La_2Ni_7 alloy, the maximum discharge capacity increases and the cycle stability improves by adding the right amount of Sc content (x = 0.3~0.5). Especially when x = 0.5, the cycle stability (S_{100}) is up to 92.6% which is obviously superior to A_2B_7-type and AB_5 type hydrogen storage alloys. We hope that our experimental results can develop the novel La-Sc-Ni-based hydrogen storage alloys by tuning their superlattice structures.

1. INTRODUCTION

Recently, ternary La-Mg-Ni compounds have been developed from corresponding binary La-Ni compounds [1, 2]. The La-Mg-Ni system has attracted extensive attention which is motivated for both fundamental interests and potential applications [3, 4]. However, the inferior cycle stability in alkaline electrolyte has been restricted their wide application [5].

The fast capacity degradation of La-Mg-Ni-based alloy electrodes could be divided into three sequential stages: 1) pulverization and Mg oxidation stage, 2) Mg and rare earth oxidation stage, and 3) oxidation-passivation stage [2, 6]. It can be concluded that the degradation process is mainly attributed to pulverization and oxidation/corrosion. For ternary La-Mg-Ni-based alloys, the replacement of La by Mg effectively decreases the volume difference between [AB_5] and [A_2B_4] subunits and enables [AB_5] subunits to absorb hydrogen. Nevertheless, there still exists significant strains during hydrogen absorption/desorption process [7]. Many literatures [8-14] report that the partial substitution of La by Mg effectively lowers the absorption/desorption plateau, restrains the amorphization of hydrides and decreases the unit cell volume change.

Moreover, Mg is a key element to improve microstructure and electrochemical performance for La-Mg-Ni-based hydrogen storage alloy. However, among La-Mg-Ni system, Mg volatilizes more quickly because of lower melting point. Hence, the Mg substitution can induce non-stoichiometry of the alloy compositions and decrease the stability of phase structure [15]. As a result, the cycle stability of the Mg-substituted alloy is unpredictable. In order to solve these problem, strategies generally involve improving the preparation technology of the La-Mg-Ni alloys, such as inhibiting Mg volatilization [16], increasing the La/Mg ratio [17]. Based on above research, the cycle stability of the Ce_2Ni_7-type electrode alloy $Mm_{0.83}Mg_{0.17}Ni_{3.1}Al_{0.2}$ is better than the commercial AB_5-type alloy, but the discharge capacity is slightly low as 340 mAh g^{-1} [3]. Furthermore, overall electrochemical performance of La-Mg-Ni-based hydrogen storage alloy still needs to be improved.

Scandium is a diagonal element of Magnesium in the periodic table and has similar chemical property with Magnesium. Meanwhile, Sc is a lighter element among lanthanide. Mei [18] shows that the work of La-Sc-Ni-based system in the same field to look into alternatives to the La-Mg-Ni system. Moreover, Sc is a key rare earth element to improve the gas hydrogen storage performance of the alloys. The investigations of ScM_2 (M = Fe, Co and Ni) alloys by Yoshida [19] demonstrates that ScM_2 Laves phase alloys could adsorb hydrogen at room temperature and its crystal structure remains stable during the hydrogenation process. Li [20] illustrates that the activation performance, the hydrogen storage capacity and the hysteresis factor of $ScMn_2$ metal hydride alloy is better than that of ScM_2 (M = Fe, Co and Ni), especially its reversible hydrogen capacity is 2.41 wt% at 298K. On the other hand, Sc is seldom used to improve the electrochemical properties of La-Sc-Ni-based hydrogen storage alloys. Therefore, it is significant to study the effects of Sc on the structure and the cycle stability of the La-Sc-Ni alloys.

In this study, the alloys with chemical composition of $La_{1-x}Sc_xNi_{3.5}$ (x = 0.0~1.0) were prepared and the effects of Sc substitution on microstructure, phase component, thermodynamic properties and electrochemical properties of $La_{1-x}Sc_xNi_{3.5}$ (x = 0.0~1.0) compounds were systematically investigated.

2. EXPERIMENTAL DETAILS

2.1 Sample Preparation

The nominal composition of the investigated alloys were $La_{1-x}Sc_xNi_{3.5}$ (x = 0~1.0). The experimental alloys were prepared by arc melting approach at 0.4 MPa of Ar atmosphere. Both of 5

wt.% La and Sc were used to compensate for evaporative loss during the melting. Then, the ingots were annealed for a week at 1173 K under Ar pressure (0.1 MPa). The purity of all elements was above 99 wt.%.

2.2 Structural and Electrochemical Characterization

Some of the annealed alloys were mechanically crushed into alloy powders, which were captured between particle size of 54 to 61 μm for electrode tests and less than 38 μm for x-ray diffraction (XRD) measurements. XRD data was collected by step-scanning method using a Rigaku D/max-2400 diffractometer with Cu radiation and a power of 40 kV×150 mA. The 2θ range of the samples was from 15 to 90°, with a step interval of 0.02°. A scanning electron microscope (SEM, JSM-5000LV) with energy dispersive spectroscopy (EDS) was used for morphological characterization and chemical analysis of the investigated alloys.

All test electrodes were prepared by cold pressing a mixture of 0.1 g alloy powers and 0.3 g carbonyl nickel power to form a pellet of 10mm in diameter under 20 MPa pressure. The electrochemical measurements were tested by a standard open tri-electrode electrolysis cell at room temperature, consisting of an alloy electrode, a sintered $Ni(OH)_2$/NiOOH counter electrode and a Hg/HgO reference electrode. The electrolyte was 6 M KOH aqueous solution. The cut-off potential was set at -0.6 V vs. Hg/HgO reference electrode in discharge process. Electrodes were charged/discharged at 60 mA g^{-1} in activated process, and at 300 mA g^{-1} when examined for cycle stability at 298 K.

2.3 Hydrogen Absorption and Desorption

Hydrogenation properties of the alloys were measured by the determination of the pressure-composition-isotherm (PCI) curves using a Sieverts-type apparatus, Beijing Nonferrous Metal Research Institute, with pressures between 0.0005 ~ 4.5 MPa at 298 K, 318 K and 343 K, respectively. Prior to formal measurements, 100 mg powder samples were evacuated at 298 K and 10^{-4} Pa for at least 2 hr in resistance furnace to remove the impurities. Then, the x = 0 alloy was measured the determination of the pressure-composition-isotherm (PCI) curves with pressures between 0.0005 ~ 4.5 MPa at 298 K and the other alloys were hydrided under 4.5 MPa and dehydrided under primary vacuum at 298 K for three times.

3. RESULTS AND DISCUSSION

3.1 Alloy crystal structure

Fig. 1 shows the XRD patterns for $La_{1-x}Sc_xNi_{3.5}$ (x = 0~1.0) alloys. The main phases for x = 0 consist mainly of La_2Ni_7 (Ce_2Ni_7-type, SG: $P6_3$/mmc) phase, $LaNi_5$ ($CaCu_5$-type, SG: P6/mmm) phase and minor LaNi phase. From Fig. 1, it can be found that the phase structure of the alloys changes obviously as Sc content increasing. Diffraction peaks gradually disappear at 2θ = 30° and 34° respectively, which indicate that $LaNi_5$ ($CaCu_5$-type, SG: P6/mmm) phase gradually disappear as Sc

content increasing. The strongest diffraction peak at $2\theta = 42^\circ$ gradually moves to the large angle. These experimental results show that La_2Ni_7 phase firstly changes to $(La, Sc)_2Ni_7$ phase, and then to Sc_2Ni_7 phase while Sc content gradually increasing. The strongest diffraction peak appears at $2\theta = 44^\circ$ for $x = 1.0$, which demonstrates that La_2Ni_7 phase completely translates to Sc_2Ni_7 phase. Based on the above analysis, the crystal structure of $La_{1-x}Sc_xNi_{3.5}$ seems to be different from the crystal structure of La-Mg-Ni-based alloys, which are attributed to the following reaction: $2(La, Mg)_2Ni_7 \rightarrow 3(La,Mg)Ni_3 + LaNi_5$. As a result, $(La,Mg)Ni_3$ phase contains more Mg content with increasing Mg content [20].
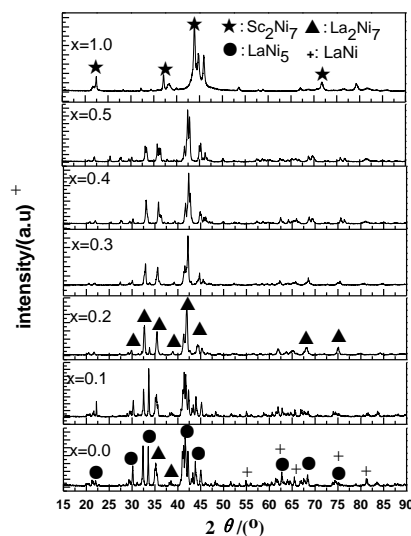

Figure 1. XRD patterns for $La_{1-x}Sc_xNi_{3.5}$ (x = 0.0, 0.1, 0.3, 0.4, 0.5, 1.0) alloys

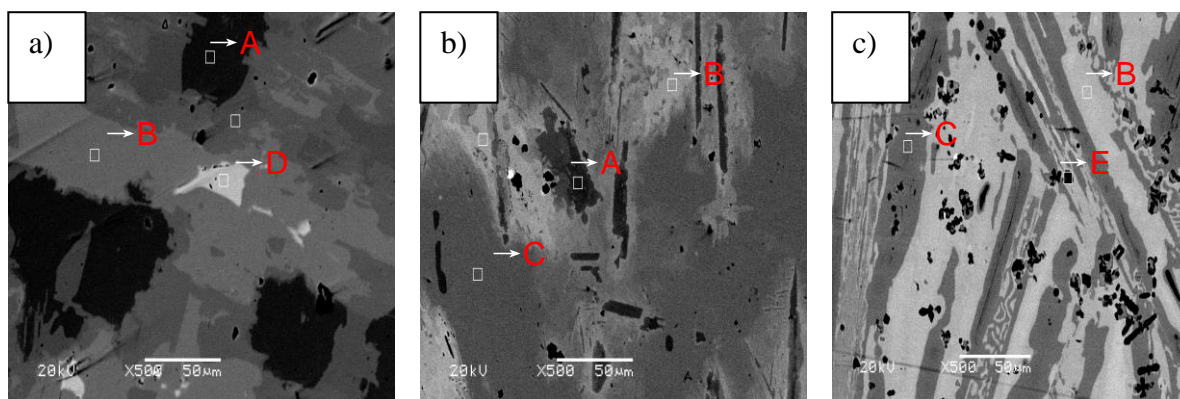**Figure 2.** Back scattered electron images for $La_{1-x}Sc_xNi_{3.5}$ alloys: a) x = 0.0, b) x = 0.3, c) x = 0.5: (A: $LaNi_5$ phase, B and C: $(La,Sc)_2Ni_7$ phase, D: LaNi phase, E: Sc_2Ni_7 phase)

The back scattered electron (BSE) images of $La_{1-x}Sc_xNi_{3.5}$ (x = 0~1.0) are shown in Fig. 2 and the relative chemical composition of different areas which were analyzed by EDS are summarized in Table 1. The different contrast regions in SEM images represent various phase types. By means of changing different areas, the mechanism of the phase formation and the variation trend of the phase aboundance can be inferred. From Fig. 2 and Table 1, it can be seen that the areas of A region (represents $LaNi_5$-type phase) and D region (represents LaNi-type phase) decrease as Sc content increasing, and disappear when $x \geq 0.5$; the areas of B and C regions (represents A_2B_7-type phase)

become the main region when x ≥ 0.3, then reach maximum when x = 1.0 (E area, represents Sc_2Ni_7-type phase). Furthermore, the relative chemical composition of B region contains less Sc than C region, which are consistent with those obtained from XRD.

Table 1. Characteristics of phases for $(La_{1.66}Mg_{0.34})Ni_7$ and $La_{0.63}R_{0.2}Mg_{0.17}Ni_{3.1}Co_{0.3}Al_{0.1}$ alloys.

Sample	Phase area	Phase composition / at%			Stoichiometric
		La	Sc	Ni	B/A
x = 0	A area/$LaNi_5$	17.39	0	82.61	4.75
	B area/La_2Ni_7	21.53	0	78.47	3.64
	D area/LaNi	48.7	0	51.3	1.05
x = 0.3	A area/$LaNi_5$	18.86	0.55	80.59	4.27
	B area/$(La,Sc)_2Ni_7$	15.67	7.82	76.51	3.26
	C area/$(La,Sc)_2Ni_7$	10.71	10.11	79.18	3.80
x = 0.5	B area/$(La,Sc)_2Ni_7$	18.66	5.69	75.65	3.11
	C area/$(La,Sc)_2Ni_7$	11.48	10.07	78.45	3.64
	E area/ Sc_2Ni_7	0.8	21.48	77.72	3.49

3.2 Thermodynamic (P-C isotherm) measurements

Fig. 3 shows hydrogen absorption/desorption P-C isotherm curves of $La_{1-x}Sc_xNi_{3.5}$ (x = 0.0, 0.1, 0.3, 0.5) measured at 298K, and Table 2 summarizes the desorption characteristics of different alloys. As far as the $LaNi_{3.5}$ alloy is concerned, the hydrogen absorption/desorption plateau goes up to 0.29 and 0.15 MPa, respectively. So the $LaNi_{3.5}$ alloy is inappropriate for hydride electrode of Ni/MH batteries. Furthermore, it is worthwhile to note that the hydrogen absorption/desorption plateaus of $La_{1-x}Sc_xNi_{3.5}$ were much lower than those of $LaNi_{3.5}$. As the Sc content increases, the hydrogen storage capacity and the hydrogen absorption/desorption plateau become distinct, and the characteristics of hydrogen absorption/desorption are listed in Table 2. It can be seen that the hydrogen capacity increases from 0.595 wt% (x = 0.1) to 1.318 wt% (x = 0.5). As Sc content increasing, the plateau pressure of hydrogen absorption/desorption firstly decreases from 0.3/0.2 atm (x = 0.1) to 0.2/0.04 atm (x = 0.3) and then increases to 0.6/0.31 atm (x = 0.5). It is worthy of noting that in Fig. 3, the P-C isotherm curves of the $La_{1-x}Sc_xNi_{3.5}$ (x ≤ 0.5) alloys show two hydrogen absorption/desorption plateaus, which is probably attributed to the different phases between the $LaNi_5$-type phase and (La, $Sc)_2Ni_7$–type phase. For example, the first absorption/desorption plateaus (the higher ones) may be originated from $LaNi_5$-type phase while the second ones (the lower ones) may be originated from (La, $Sc)_2Ni_7$–type phase for x = 0.1 and 0.3. Comparing with the $LaNi_5$-type phase, the latter provides more available interstices for H in the lattice, which can lower the hydrogen absorption/desorption plateau pressures of the (La, $Sc)_2Ni_7$–type phase. As described above, it indicates that the addition of Sc element can lower the hydrogen absorption/desorption plateaus and improve reversible ability of hydrogen absorption/desorption process.
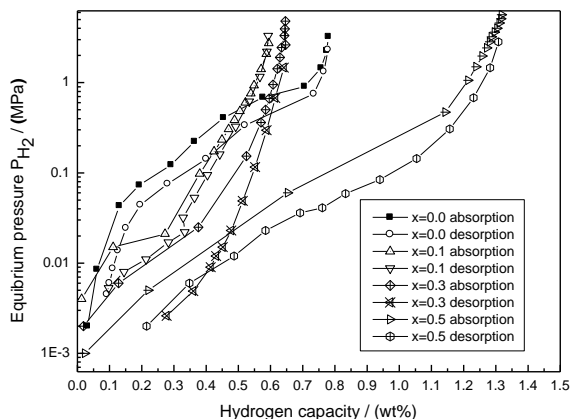
Figure 3. P-C isotherms of La$_{1-x}$Sc$_x$Ni$_{3.5}$ (x = 0.0, 0.1, 0.3, 0.5) alloys at 298K

Table 2. Hydrogen desorption characteristics for La$_{1-x}$Sc$_x$Ni$_{3.5}$ annealed alloys at 298K

Alloy	Hydrogen capacity (wt%)	Pa (atm)	Pd (atm)	Hysteresis factor[*]
x = 0.0	0.78	2.8	1.5	0.62
x = 0.1	0.595	0.3	0.2	0.41
x = 0.3	0.647	0.2	0.04	1.61
x = 0.5	1.318	0.6	0.31	0.66

Note: P$_a$ and P$_d$ are the pressure at midpoint of absorption/desorption hydrogen process. Hysteresis factor[*] = Log(P$_a$/P$_d$)

The pressure-composition-temperature (P-C-T) curves of the La$_{1-x}$Sc$_x$Ni$_{3.5}$ (x = 0.1, 0.3) alloy samples measured at 298 K, 318 K and 343 K are shown in Fig. 4(a)-(b). It can be seen that when log P$_{eq}$ (equilibrium plateau pressure) at midpoint of hydrogen storage capacity are plotted against 1/T according to the following expression, the desorption plateau appears a linearity in the van't Hoff plot for the La$_{1-x}$Sc$_x$Ni$_{3.5}$ system.
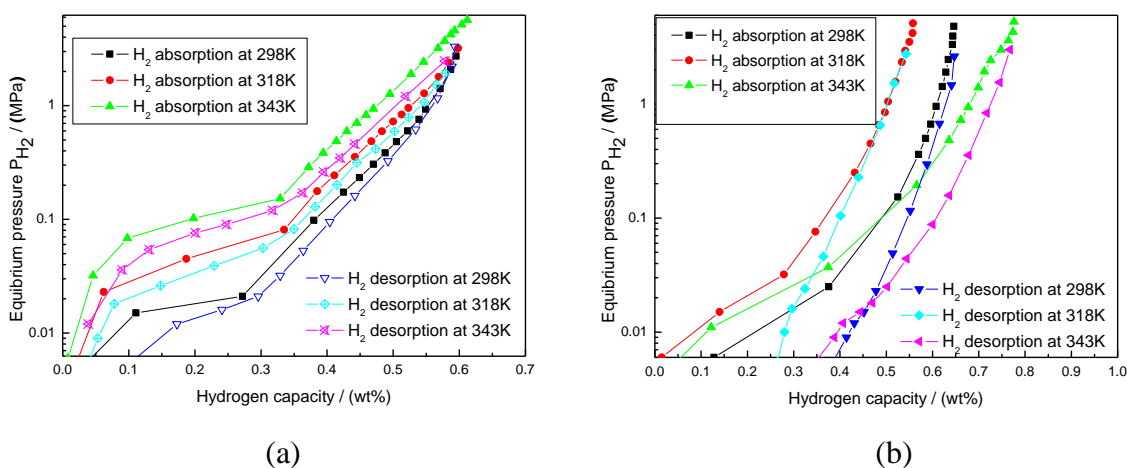

(a)

(b)

Figure 4. P-C-T curves of La$_{0.9}$Sc$_{0.1}$Ni$_{3.5}$ (a), La$_{0.7}$Sc$_{0.3}$Ni$_{3.5}$ (b) alloys at 298K, 318K and 343K

(A) Van't Hoff equation

$$\ln P = (\Delta H/RT) - (\Delta S/R) \tag{1}$$

(B) Van't Hoff plot of $La_{0.9}Sc_{0.1}Ni_{3.5}$ alloy in Fig. 5, absorption

$$\ln P(atm) = -5.6689/T + 16.5679$$

(2)

The enthalpy change (ΔH) and entropy change (ΔS) for H_2 absorption reaction corresponding to E_{qs}. (1) and (2) are $\Delta H = -11.3$ (kcal mol^{-1}) and $\Delta S = 32.9$ (cal mol$^{-1} \cdot K^{-1}$)

(C) Van't Hoff plot of $La_{0.9}Sc_{0.1}Ni_{3.5}$ alloy in Fig. 5, desorption

$$\ln P(atm) = -5.1769/T + 12.5156$$

(3)

The enthalpy change (ΔH) and entropy change (ΔS) for H_2 desorption reaction from E_{qs}. (1) and (3) are $\Delta H = -10.3$ (kcal mol^{-1}) and $\Delta S = 24.87$ (cal mol$^{-1} \cdot K^{-1}$).

Then, in a similar way, (D) Van't Hoff plot of $La_{0.7}Sc_{0.3}Ni_{3.5}$ alloy in Fig. 5, absorption

$$\ln P(atm) = -3.5170/T + 8.7471$$

(4)

The enthalpy change (ΔH) and entropy change (ΔS) for H_2 absorption reaction corresponding to E_{qs}. (1) and (4) are $\Delta H = -7.0$ (kcal mol^{-1}) and $\Delta S = 17.38$ (cal mol$^{-1} \cdot K^{-1}$)

(E) Van't Hoff plot of $La_{0.7}Sc_{0.3}Ni_{3.5}$ alloy in Fig. 5, desorption

$$\ln P(atm) = -3.1769/T + 7.5156$$

(5)

The enthalpy change (ΔH) and entropy change (ΔS) for H_2 desorption reaction from E_{qs}. (1) and (5) are $\Delta H = -6.3$ (kcal mol^{-1}) and $\Delta S = 14.93$ (cal mol$^{-1} \cdot K^{-1}$).

It is clear that the hydride formation enthalpy of the alloy ($x = 0.1$) is far larger than AB_5 systems while the hydride formation enthalpy of $x = 0.3$ is similar to the exothermic process observed in the AB_5 systems. Hence, as Sc content increasing, the partial substitution of La by Sc remarkably lowers the hydride formation enthalpy of $LaNi_{3.5}$ alloy. However, it is worthwhile to note that, in Table 2, the hysteresis factor of the $La_{0.5}Sc_{0.5}Ni_{3.5}$ is much smaller than $La_{0.7}Sc_{0.3}Ni_{3.5}$, indicating that the $La_{0.5}Sc_{0.5}Ni_{3.5}$ has a better hydriding/dehydriding cyclic stability than $La_{0.7}Sc_{0.3}Ni_{3.5}$. This phenomenon testifies that the La-Sc-Ni-type structure is also a good host for H_2.

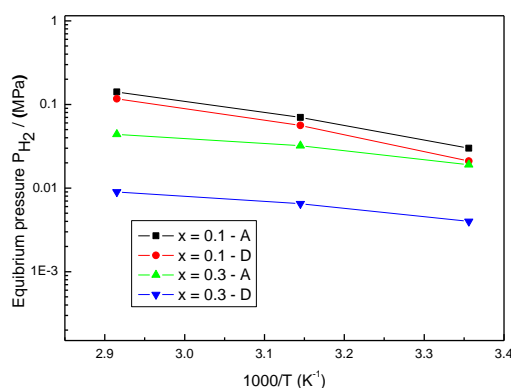**Figure 5.** Van't Hoff plots of $La_{1-x}Sc_xNi_{3.5}$-H ($x = 0.1, 0.3$) hydrogen storage alloy

3.3 Charge/discharge characteristics

Fig. 6 shows the activation curves of $La_{1-x}Sc_xNi_{3.5}$ (x = 0.0, 0.1, 0.3, 0.4, 0.5, 1.0) alloy electrodes, and Table 3 summarizes the electrochemical performance of different alloy electrodes. It can be found that all of alloy electrodes exhibited good activation properties except x ≥ 0.5; three charge/discharge cycles were enough to activate electrodes. Meanwhile, the maximum discharge capacity increases firstly from 232.7 mAh g^{-1} (x = 0.0) to 285.1 mAh g^{-1} (x = 0.4) and then gradually decreases to 28.7 mAh g^{-1} (x = 1.0) with the increase of Sc content. This phenomenon may be attributed to the variation of the phase structure for the alloys. With increasing the Sc content, the phase abundance of $(La, Sc)_2Ni_7$ and Sc_2Ni_7 phases increase, as well as $LaNi_5$ phase decreases. When Sc content $\geqslant$ 0.5, Sc_2Ni_7 phase becomes main phase and the discharge capacity is rather low because Sc_2Ni_7 phase is difficult to absorb H_2.
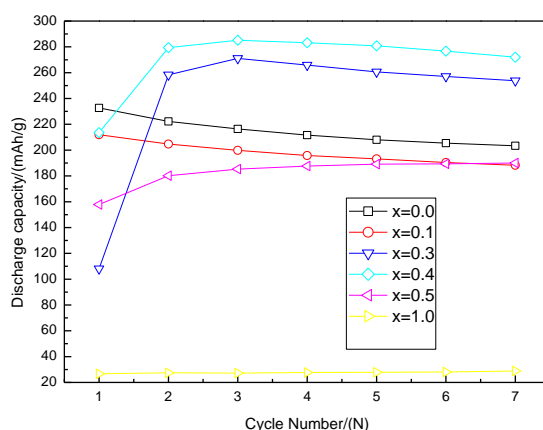

Figure 6. Activation curves of $La_{1-x}Sc_xNi_{3.5}$ (x = 0.0, 0.1, 0.3, 0.4, 0.5, 1.0) annealed alloy electrodes with 60mA g^{-1} charge-discharge current density at 298K

Table 3. Summary of electrochemical performance for $La_{1-x}Sc_xNi_{3.5}$ annealed alloy electrodes at 298K

Sample	N	C_{max}(mAh g^{-1})		S_{100}(%)
		60 mA g^{-1}	300 mA g^{-1}	
x = 0.0	1	232.7	185.3	60.6
x = 0.1	1	211.9	169.8	65.3
x = 0.3	3	271.1	178.0	67.8
x = 0.4	3	285.1	211.6	74.6
x = 0.5	7	190	177.5	92.6
x = 1.0	7	28.7	12.3	63.4

As we know, Mg plays a quite important role in hydrogen storage behavior for La-Mg-Ni-based hydrogen storage alloys. By adding proper amount of Mg, the hydrogen-induced amorphization can be reduced and the cycle stability of the alloys can be improved [21].

The effect of Sc on La-Sc-Ni-based alloys is similar to Mg in the La-Mg-Ni systems. Furthermore, from the thermodynamic point of view, the enthalpy for H_2 absorption/desorption reaction of $La_{0.7}Sc_{0.3}Ni_{3.5}$ is -7.0/-6.3 kcal mol^{-1}, which is similar to the $La_{1.66}Mg_{0.34}Ni_7$-H_2 system (-7.5 kcal mol^{-1}) [12]. When the Sc content further increase, the plateau pressure of x = 0.5 increases to 0.6/0.31 atm in Table 2, respectively. As a consequence, the lower plateau pressure lead to the alloy is difficult to absorp/desorp H_2, and result in the lower discharge capacity.
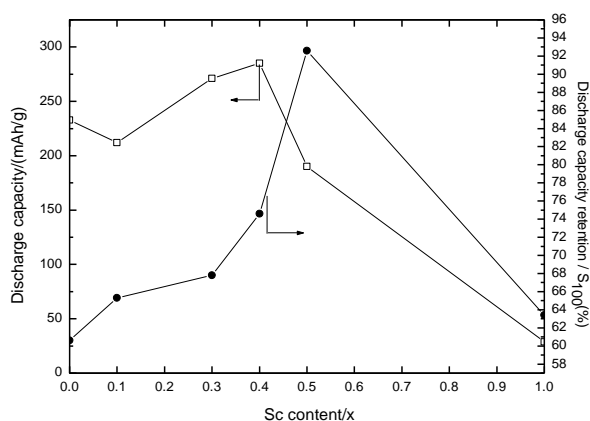
3.4 Cyclic stability

Figure 7. Discharge capacity and cycle life of $La_{1-x}Sc_xNi_{3.5}$ annealed alloy electrodes as a function of Sc content (x)
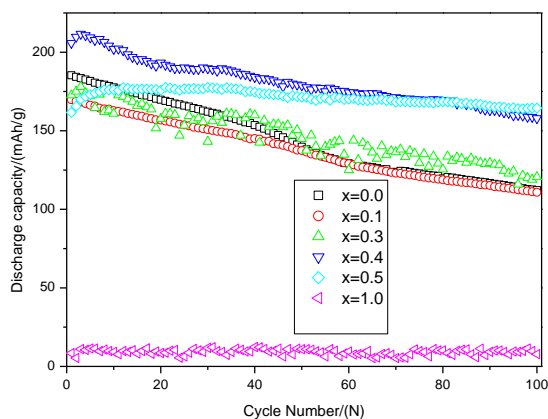

Figure 8. Cyclic stability curves of $La_{1-x}Sc_xNi_{3.5}$ annealed alloy electrodes with 300mAg^{-1} charge-discharge current density at 298K

Figs. 7 and 8 show the discharge capacity retention curves of $La_{1-x}Sc_xNi_{3.5}$ (x = 0.0, 0.1, 0.3, 0.4, 0.5, 1.0) alloy electrodes. It can be found that the cycle stability of all alloy electrodes decreases gradually as cycle number increasing. In order to illustrate cycle stability, capacity retention rate at the 100th cycle (S_{100}) is calculated as the ratio of C_{100}/C_{max}, and is listed in Table 3. It can be seen that the

cycle stability of the alloy electrodes initially increases from 60.6% (x = 0.0) to 92.6% (x = 0.5) and then drops to 63.4% (x = 1.0). The discharge capacity degradation of the alloy electrodes is closely correlated with the pulverization of the alloy particles, the corrosion of the alloy active component in alkaline electrolyte and the amorphous tendency of the alloys during charging/discharging process [22, 23].

The following reasons are responsible for the improvement of the cycle stability for the alloys by substituting La with Sc. Firstly, the positive impact of Sc substitution is attributed to the refinement of the grains. When hydrogen atoms enter into the interstitial sites of the lattice, the lattice stress and the expansion of the cell volume for the alloys both inevitably increase, which result in the pulverization of the alloy. The Sc substitution prominently refine the grains of the alloys, which efficiently improve the anti-pulverization capability of the hydrogen storage alloys. Secondly, it should be noticed that the $LaNi_5$ phase of the alloys is gradually disappear. At the same time, the phase abundance of $(La, Sc)_2Ni_7$ phase originated from substituting La with Sc gradually increases for improving the cycle stability of the alloy as Sc content rising. Thirdly, according to the XRD patterns (Fig. 1), it is known that as Sc content increasing, the strongest diffraction peaks gradually move to the large angle. This results indicated that La is partially substituted by Sc while the atomic percent of La decreases and that of Sc increases equally. Therefore, the amorphous tendency of Sc-containing alloy hydrides are restrained to some extent because the atomic radius of Sc (164 pm) is smaller than that of La (187.7 pm). The value of the average A-atomic radius (r_A) / the average B-atomic radius (r_B) does not meet the 1.37 standards [24]. Moreover, Ce (-2.336 V) is just slightly less-oxidizable than La (-2.379 V) and it is well-known that partial substituting La with Ce can reduce the oxidation in KOH. Similarly, Sc has a much higher half-cell potential (-2.077 V) and should make contribution to the oxidation-resistance. Therefore, during charge/discharge process, Sc addition can inhibit the amorphous tendency of the alloys.

Based on the above analysis, it can be concluded that a proper amount substitution (x = 0.4~0.5) of Sc for La can improve the cycle stability of the alloys, which is attributed to the better anti-pulverization capability and the lower amorphous tendency. Nevertheless, with further increase of Sc content, the discharge capacity decreases and the cycle stability deteriorates for the alloys.

4. CONCLUSIONS

The structure and electrochemical properties of different Sc-substituted alloys have been studied systematically. Some conclusions can be summarized:

1) The XRD patterns and SEM–EDS analyses show that the original Sc-free alloy consists of two major phase: $LaNi_5$ phase, La_2Ni_7 phase, and LaNi minor phase. A range of Sc addition (x = 0.3~0.5) increases the abundance of $(La, Sc)_2Ni_7$-type phase while that of $LaNi_5$ and LaNi phases decrease. Moreover, with continuous increase of Sc content, the Sc_2Ni_7 phase appears. Hence, the crystal structure of La-Sc-Ni systems seems to be different from the crystal structure of La-Mg-Ni-based alloys.

2) The thermodynamic properties indicate that Sc-containing alloy has a lower absorption/desorption plateau than those of LaNi$_{3.5}$, and hydrogen storage capacity increases from 0.595 wt% (x = 0.1) to 1.318 wt% (x = 0.5) as Sc increasing. Meanwhile, the absolute values of enthalpy variations ($|\Delta H|$) during hydrogen absorption/desorption process decrease from 11.3/10.3 kcal mol^{-1} to 7.0/6.3 kcal mol^{-1} with increasing Sc content, which indicate that a proper amount of Sc addition alloy is also a good host for H$_2$. However, the equilibrium absorption/desorption hydrogen pressure plateau is still higher than La-Mg-Ni systems, which result in poor discharge capacity during electrochemical measurement.

3) A range of Sc addition (x = 0.3~0.5) results in the increase of maximum discharge capacity and the improvement of cycle stability for the alloy electrodes which can be ascribed to the increase of (La, Sc)$_2$Ni$_7$–type phase and the addition of Sc suppresses the amorphization of the LaNi$_{3.5}$ alloy of the alloy electrodes. The findings in this work are expected to inspire research on developing the novel La-Sc-Ni-based hydrogen storage alloys and the improvement of the electrochemical properties of La-Sc-Ni-based alloys from optimizing the composition, constituent phase structures and thermodynamic parameters of the superlattice alloys.

References

1. K. T. Moller, T. R. Jensen, E. Akiba, and H. W. Li, *Progress in Natural Science:Materials International,* 27 (2017) 34.
2. Z. J. Gao, and H. M. Zhang, *Int. J. Electrochem. Sci.*, 11 (2016) 1282.
3. S. Yasuoka, Y. Magari, T. Murata, T. Tanaka, J. Ishida, H. Nakamura, T. Nohma, M. Kihara, Y. Baba, and H. Teraoka, *J. Power Sources,* 156 (2006) 662.
4. J. J. Liu, Y. Li, S. M. Han, S. Q. Yang, W. Z. Shen, X. C. Chen, and Y. M. Zhao, *J. Electrochem Soc.,* 160 (2013) A1139.
5. Y. M. Zhao, S. M. Han, Y. Li, J. J. Liu, L. Zhang, and S. Q. Yang, *Electrochim. Acta,* 152 (2015) 265.
6. R. F. Li, J. Wan, F. Wang, C. P. Ding, and R. H. Yu, *J. Power Sources,* 301 (2016) 229.
7. Y. Nakamura, J. Nakamura, K. Iwase, and E. Akiba, *Nucl. Instrum. Meth. A,* 600 (2009) 297.
8. A. Ferey, F. Cuevas, M. Latroche, B. Knosp, and P. Bernard, *Electrochim. Acta,* 54 (2009) 1710.
9. J. Nakamura, K. Iwase, H. Hayakawa, Y. Nakamura, and E. Akiba, *J. Phys Chem. C,* 113 (2009) 5853.
10. R. V. Denys, A. B. Riabov, R. Černý, I. V. Koval'chuk, and I. Yu. Zavaliy, *J. Solid State Chem.,* 187 (2012) 1.
11. R. V. Denys, A. B. Riabov, V. A. Yartys, M. Sato, and R. G. Delaplane, *J. Solid State Chem.,* 181 (2008) 812.
12. M. N. Guzik, B. C. Hauback, and K. Yvon, *J. Solid State Chem.,* 186 (2012) 9.
13. Z. W. Ma, D. Zhu, C. L. Wu, C. L. Zhong, Q. N. Wang, W. H. Zhou, L.S. Luo, Y.C. Wu, and Y. G. Chen, *J. Alloys Compd.,* 620 (2015) 149.
14. J. J. Liu, S. M. Han, D. Han, Y. Li, S. Q. Yang, L. Zhang, and Y. M. Zhao, *J. Power Sources,* 287 (2015) 237.

15. K. L. Lim, Y. N. Liu, Q. A. Zhang, K. S. Lin, and S. L. I. Chan, *J. Alloys Compd.,* 661 (2016) 274.
16. W. Zhu, C. Tan, J. B. Xu, and Z. X. Li, *J. Electrochem Soc.,* 161 (2014) A89.
17. L. Zhang, W. K. Du, S. M. Han, Y. Li, S. Q. Yang, Y. M. Zhao, C. Wu, and H. Z. Mu, *Electrochim. Acta,* 173 (2015) 200.
18. X. Z. Mei, Y. C. Luo, G. Q. Zhang, and L. Kang, *J. Inorganic Materials,* 30 (2015) 1049.
19. M. Yoshida, and E. Akiba, *J. Alloys Compd.,* 226 (1995) 161.
20. W. H. Li, B. H. Tian, P. Ma, and R. D. Wu, *Acta Metallurgica Sinica,* 48 (2012) 822.
21. Z. J. Gao, Y. C. Luo, R. F. Li, Z. Lin, and L. Kang, *J. Power Sources,* 241 (2013) 509.
22. K. Young, T. Ouchi, L. Wang, and D. F. Wong, *J. Power Sources,* 279 (2015) 172.
23. L. Zhang, Y. Q. Ding, Y. M. Zhao, Du W. K., Y. Li, S. Q. Yang, and S. M. Han, *Int. J Hydrogen Energy,* 41 (2016) 1791.
24. J. Zhang, F. Fang, S. Y. Zheng, J. Zhu, G. R. Chen, and D. L. Sun, *J. Power Sources,* 172 (2007) 446.